A&A 426, 309–322 (2004)
DOI: 10.1051/0004-6361:20040456


Astronomy & Astrophysics

# MAFAGS-OS: New opacity sampling model atmospheres for A, F and G stars

## II. Temperature determination and three "standard" stars

F. Grupp

Universitäts Sternwarte München, Scheinerstr. 1, 81679 München, Germany
e-mail: fug@usm.uni-muenchen.de

Received 16 March 2004 / Accepted 17 June 2004

**Abstract.** The influence of the new MAFAGS-OS opacity sampling model atmosphere and its changed thermal structure is tested on two of the major methods to determine stellar effective temperatures: the *infrared flux method* and the *Balmer line method*. Both methods are shown to be affected by the new model. How a change of the resonance broadening theory according to Ali & Griem (1965) improves the theoretical Balmer line spectrum of the Sun is studied.
The new model together with the modified resonance broadening cross sections for hydrogen are then applied to three stars: Procyon, Groombridge 1830 and HD 19445. Stellar parameters measured for these stars lead to new determinations of masses, ages and spectroscopic distances for these objects. While Procyon's parameters are only slightly changed with respect to recent ODF-based analyses, the temperatures of Groombridge 1830 and HD 19445 are significantly increased, leading to higher masses and lower ages for these two stars. Compared to ODF-based studies, the paradox of Groombridge 1830 and HD 19445 having ages well above the *age of the Universe* is resolved and the determined spectroscopic parallaxes are in very good agreement with high precision Hipparcos astrometry.

**Key words.** methods: numerical – stars: individual: Procyon – stars: individual: Groombridge 1830 – stars: individual: HD 19445 – stars: atmospheres – Sun: fundamental parameters

## 1. Introduction

In Paper I (Grupp 2004) we have shown the basic principles and input physics of our new *opacity-sampling* (OS) model atmosphere calculation code MAFAGS-OS. This new model was compared to empirical models, *opacity-distribution-function* (ODF) and other OS models. The direct comparison to the corresponding ODF model showed a temperature structure $T(\tau)$ of MAFAGS-OS up to 60 K hotter than MAFAGS-ODF. This increased temperature will affect both *infrared flux method* and *Balmer-line* temperature determination. Temperature structures of the ODF and the OS model are displayed in Fig. 1. The influence of this changed temperature structure on these two methods will be studied in detail in this paper.

The ODF and the OS version of MAFAGS use different sources of Fe I bound-free opacities. Whilst MAFAGS-ODF is calculated based on a simple hydrogen approximation, MAFAGS-OS uses new calculations of Bautista (1997). These new cross-sections that produce a significantly higher ultraviolet opacity lead to a redistribution of flux to the infrared spectral region as shown in Paper I.

Fuhrmann et al. (1993), Fuhrmann (1993) and Bernkopf (1998) showed that the ODF version of our code fits the observed Balmer-line spectrum of the Sun within 20 K limits.

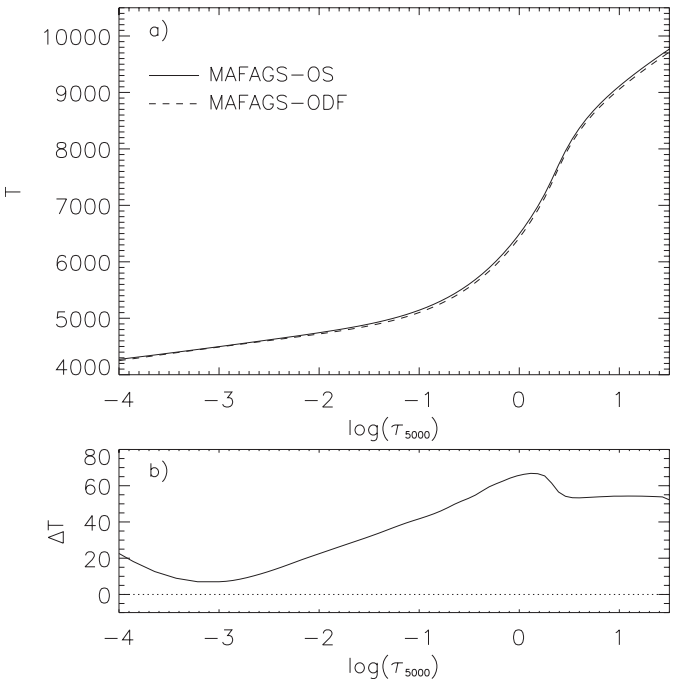


**Fig. 1.** Temperature structure of the MAFAGS-OS and MAFAGS-ODF solar model. **b)** Difference between OS and ODF model.

**Table 1.** Basic data and observational properties for our standard stars. Common name, Henry Draper catalogue number, HIPPARCOS catalogue number, visual brightness, date of observation, spectral resolution, exposure time, signal to noise at $H_\alpha$, $H_\beta$, $H_\gamma$.

| Name | HD | Hip | $V$ [mag] | Date | $\Delta\lambda/\lambda$ | $T_{\rm exposure}$ [s] | $S/N(H_\alpha)$ | $S/N(H_\beta)$ | $S/N(H_\gamma)$ |
|---|---|---|---|---|---|---|---|---|---|
| Procyon | 61421 | 37279 | 0.34 | Jan. 30.2001 | 60 000 | 40 | 448 | 321 | 236 |
| Groombridge 1830 | 103095 | 57939 | 6.45 | May 19.2000 | 60 000 | 900 | 356 | 200 | 120 |
| – | 19445 | 14594 | 8.05 | Dec. 24.1999 | 60 000 | 3000 | 290 | 190 | 126 |

Their result, and the fact that an increased temperature structure will affect this fit, will be treated in detail in Sect. 3.

Furthermore, the new model MAFAGS-OS that was shown to reproduce the solar flux distribution and UBV colors will have to face three so-called *"standard" stars*[1]. We have chosen the three stars Procyon, Groombridge 1830 and HD 19445 as they are well known, and very different representatives of stars spread over the parameter range MAFAGS-OS is designed for. These stars are only samples and we do not claim that they cover the parameter space in any sense of completeness.

The model will be used to determine stellar parameters, and using evolutionary models, the masses and ages of the three stars.

Basic properties of observations for our three stars are given in Table 1. All observations where performed using the FOCES[2] spectrograph at the Calar Alto observatory. For an outline on the fibre coupled FOCES instrument and its properties see Pfeiffer et al. (1998) and Grupp (2003).

## 2. Infrared flux method temperatures

Proposed by Blackwell & Shallis (1977) and Blackwell et al. (1980) the so-called *infrared flux method* has become a common and extensively used method used to determine stellar diameters and effective temperatures.

The basic idea of the *infrared flux method* is the measurement of two stellar quantities that can be accessed with high accuracy: $F(\lambda)$, the flux density (in absolute values) at a given wavelength, and the total integrated stellar flux $F_{\rm bol}$. These two observed values are related to model parameters through Eq. (1).

$$R(\lambda) = \frac{F_{\rm bol}}{F(\lambda)} = \frac{\sigma T_{\rm eff}^4}{F_{\rm model}(T_{\rm eff}, \log(g), \lambda, [{\rm M/H}], ...)}. \quad (1)$$

The right hand side of Eq. (1) contains the Stefan-Boltzmann law and the theoretical, model dependant monochromatic flux $F_{\rm model}(T_{\rm eff}, \log(g), \lambda, [{\rm M/H}], ...)$, i.e. the right hand side can be calculated using theoretical atmospheric models. Comparison of those theoretical values of $R$ to measured fractions $R(\lambda)$ leads to direct measurement of the stellar effective temperature $T_{\rm eff}$. In principle this method would work for all monochromatic fluxes $F(\lambda)$. As these fluxes are expected to be least influenced by uncertainties in the opacity calculation in the according wavelength range *infrared* bands are used. Most authors use $R(\lambda)$ ratios calculated and tabulated for the infrared stellar bands $J$ ($\lambda$ = 12 725 Å), $H$ ($\lambda$ = 16 350 Å) and $K$ ($\lambda$ = 21 750 Å) and compare these data to observed $R(\lambda)$ ratios (see for example Alonso et al. (1996) or Blackwell & Lynas-Gray (1998)).

The fact that the infrared flux method is not independent of the theoretical model applied was first discussed by Megessier (1994) who found differences between different theoretical models for the obtained $T_{\rm eff}$ up to 290 K.

As shown in Paper I our solar OS model shows an increased ultraviolet opacity, reducing the so-called *missing ultraviolet opacity* problem and showing good agreement with the measured solar flux distribution in the UV. This decreased flux in the UV leads to a increased flux in the visual and infrared region, as the total flux emerging from the model star is to be conserved. This fact, that was also noticed by Megessier (1998), leads to a change of $T_{\rm eff}$ measured with the infrared flux method when changing from our ODF to our OS model. This is shown for our solar model in Fig. 2. Figures 2b–d show this comparison between the ODF and OS solar models together with a solar ODF model with an effective temperature increased by 65 K.

Because the increase of the infrared flux is connected to an increase of ultraviolet opacity that is mainly due to the use of new bound-free cross sections for Fe I determined by Bautista (1997), we can expect this effect to occur in all stars where iron I is a dominant contributer to the UV-opacity. The increase in the infrared flux will translate to a systematic *increase* of measured effective temperatures.

To give an impression of the quantitative change we present the temperature change when going from ODF to OS for the three bands $J$, $K$ and $H$ in Fig. 3 for the solar metallicity main sequence. Note that the differences in $T_{\rm eff}$ given here are only rough values, as the exact parameters of the star considered should be used instead of any standard main-sequence data.

Figure 3 shows that indeed higher infrared temperatures are measured for the three filters $J$, $H$ and $K$. The maximum difference when going from ODF to OS models is found for the main sequence stars around 6000–6500 K with $\Delta(T_{\rm eff}) \approx 55$ K or 1%. Towards higher temperatures and thus thermal energies the importance of Fe I photoionization cross sections compared to other opacity sources in the UV decreases. Therefore the difference between ODF to OS model infrared temperature decreases. It reaches <15 K at $T_{\rm eff}$ = 10 000 K.

Although there seems to be a tendency for higher deviations in $K$-band and lower ones in the $J$-band the estimated accuracy

[1] In fact almost all stars, that are claimed to be any kind of "standard" fail to keep this attribute if looked at more closely.

[2] Visiting Astronomer, German-Spanish Astronomical Centre, Calar Alto, operated by the Max-Planck-Institute for Astronomy, Heidelberg, jointly with the Spanish National Commission for Astronomy.

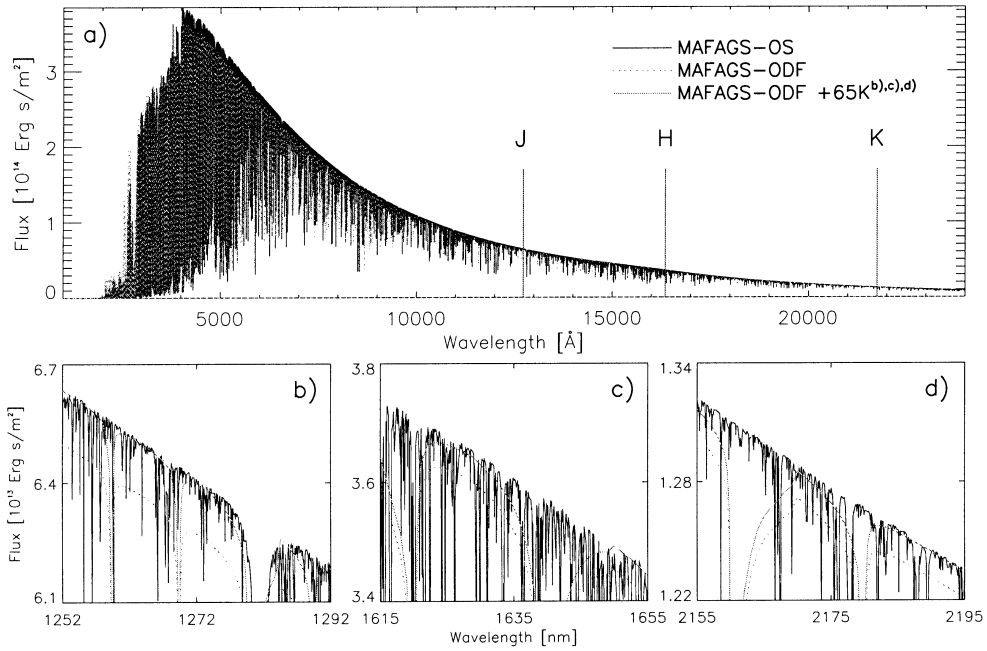


**Fig. 2.** Flux emerging from MAFAGS-OS (full, black line) and MAFAGS-ODF (dashed, grey line) solar model. The central wavelengths of the filters $J$, $H$ and $K$ are marked in **a)**. **b)–d)** wavelength range around the stated filters; in addition a MAFAGS-ODF model with 5842 K is plotted as full grey line, fitting the continuum of the OS model.

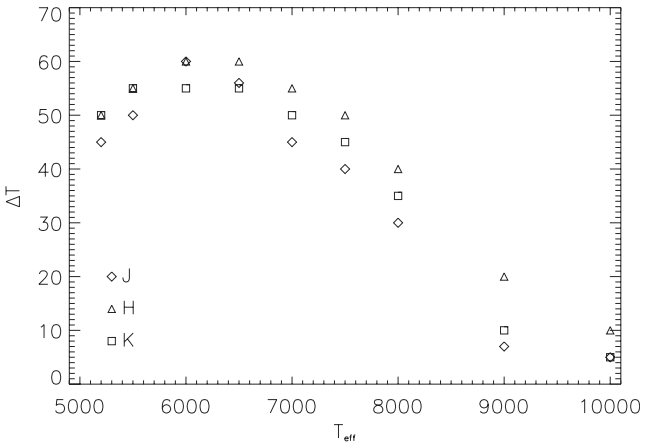


**Fig. 3.** Difference in determined infrared-flux-method temperature when turning from the MAFAGS-ODF to MAFAGS-OS model for the solar metallicity ([M/H] = 0) main sequence.

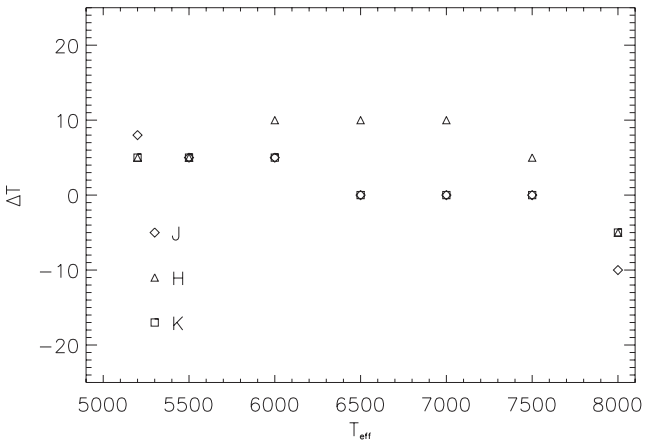


**Fig. 4.** Same as Fig. 3 but for a metal-poor ([M/H] = −2) main sequence.

of our measurements, being of the order of 10 K for all filter regions, does not allow this conclusion.

In Fig. 4 the difference between MAFAGS-ODF and MAFAGS-OS infrared temperature is plotted for a metal-poor main sequence of [M/H] = −2.0. As Fe I photo ionization plays only a minor role in metal-poor main sequence stars we expect, and find, only small differences between ODF and OS model infrared temperatures for stars with $T_{\rm eff}$ = 5000–8000 K.

## 3. Balmer-line temperatures

For a long time Balmer lines have been are successfully used to determine stellar effective temperatures. Among others Spite (1969), de Strobel (1985), Perrin et al. (1988), Cayrel de Strobel & Bentolila (1989), Fuhrmann (1993), Fuhrmann et al. (1994), Fuhrmann et al. (1997) and Korn et al. (2003) used Balmer lines for an extended sample of stars, measuring $T_{\rm eff}$.

It is evident that changes in the atmospheric structure will influence the profile of the Balmer lines and therefore the measured effective temperatures.

The influence of convection on Balmer line profiles was first studied by Fuhrmann (1993) and Fuhrmann et al. (1993). He found that the efficiency of convection, described by the parameter $\alpha_{\rm bv}$ in the Böhm-Vitense (1958) *mixing length approach*, strongly influences the higher members of the Balmer series, whereas $H_\alpha$is least affected. Knowing this, Fuhrmann used this dependency to measure the a priori unknown

efficiency of convection $\alpha_{\rm bv}$, forcing $H_\alpha \cdots H_\delta$ to produce the same solar $T_{\rm eff}$ = 5777 K. Doing this Fuhrmann et al. (1993) find $\alpha_{\rm bv} = 0.5$, i.e. a significantly less efficient convection than assumed by most previous analyses assuming $\alpha_{\rm bv} = 1.5$–$2.0$. These results and analyses were verified by Castelli et al. (1997) and Gardiner et al. (1999).

As described in detail in Paper I, we do not follow the above stated approach and treat $\alpha$ as a "free" parameter. Following Bernkopf (1998) who consistently treats stellar evolution, i.e. the stellar interior, and stellar atmospheres in the convection theory of Canuto & Mazzitelli (1991) we adopt Bernkopfs measurement of $\alpha_{\rm cm} = 0.82$. This value, fixed from stellar evolution requirements, reproduces the present Sun in its evolutionary state.

### 3.1. Balmer-line profiles

Several physical processes contribute to the final profile function $\Phi$ of the Balmer lines we are interested in.

In the process of line formation we treat the following contributers:

**Radiation broadening:** This process is based on the fact that the energy of an atomic level is subject to the Heisenberg uncertainty principle.

**Doppler broadening:** Thermal and non thermal movement of absorbing atoms lead to Doppler broadening.

**Stark broadening:** The process of linear stark-effect is accounted for using profile functions calculated according to the theory of Vidal et al. (1973) by Schöning & Butler (1990).

**Resonance broadening:** This process, based on the fact that absorbing hydrogen atoms are influenced by other neutral hydrogen atoms is accounted for in the formulation of Ali & Griem (1965).

**Microturbulence and rotational broadening:** These influences are non atomic, macroscopic effects and are considered in our model.

Whilst *radiation broadening* and *Doppler broadening* play only a minor role, the *Stark effect* and *resonance broadening* dominate the profile of the lower members of the Balmer series used to determine stellar temperatures. Figure 5 shows the influence of resonance broadening on the Balmer line profile for the Sun and a $T_{\rm eff}$ = 7000 K main sequence star. It is obvious that resonance broadening plays the most dominant role with $H_\alpha$ and its importance decreases rapidly towards the higher series members. On the other hand it can be seen that the importance of resonance broadening decreases rapidly towards higher temperatures.

There exists a completely different approach to determine Balmer line profiles. Barklem et al. (2000b), Barklem et al. (2000a) and Barklem et al. (2002) present a method using "resonance and dispersive-inductive interactions with H-atom" to calculate hydrogen profile functions. Although this approach seems rather promising they fail to reproduce the solar Balmer line spectrum (Fig. 3 in Barklem et al. 2000b, Fig. 8 in Barklem et al. 2000a and Fig. 3 in Barklem et al. 2002) and temperature (Table 4 in Barklem et al. 2002). Furthermore, the tendency to produce significantly cooler temperatures with their model results in much higher stellar ages. This effect, most dominant in solar temperature metal-poor stars (see Fig. 7 in Barklem et al. 2000a) will increase the problem of many metal-poor stars having unreasonably high ages[3].

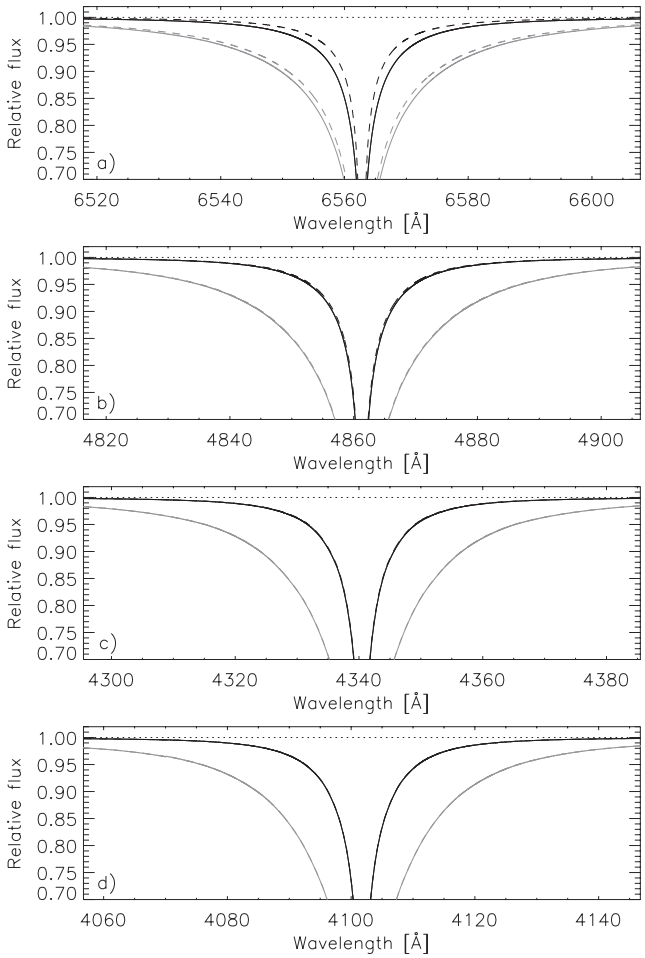


**Fig. 5.** Solar (black) and $T_{\rm eff}$ = 7000K (grey) Balmer lines $H_\alpha$ – $H_\gamma$ calculated with (full line) and without (dashed line) resonance broadening.

### 3.2. The Sun

Turning to the Sun as our major reference we have unique conditions to test our model. First we know the solar effective temperature with outstanding accuracy. Second, the Kitt Peak Solar Flux Atlas by Kurucz et al. (1984) provides spectroscopic data with high resolution.

Using the broadening mechanisms presented in 3.1 together with our MAFAGS-OS solar model we calculate the Balmer line profiles for the solar $H_\alpha$ and $H_\beta$ line. These theoretical profiles, together with Kitt Peak flux measurements, are presented in Figs. 6 and 7. Both figures show that the flux, calculated by our model, is too weak, i.e. it underpredicts the observations. A fact that can be called the *mortal sin* of line fitting. This deficiency becomes even more obvious looking at Figs. 6b and 7b,

[3] Higher than the age of the Universe as determined using $H_0$.

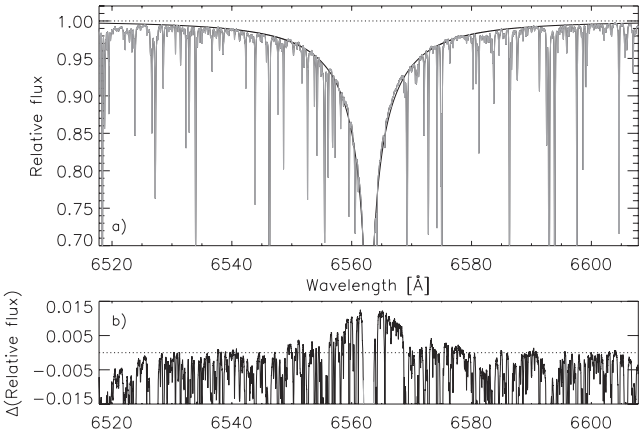


**Fig. 6.** Solar $H_\alpha$ line. Kitt Peak Solar Atlas (grey) and MAFAGS-OS prediction (black). Figure **b)** shows the relative deviation of measurement and prediction.

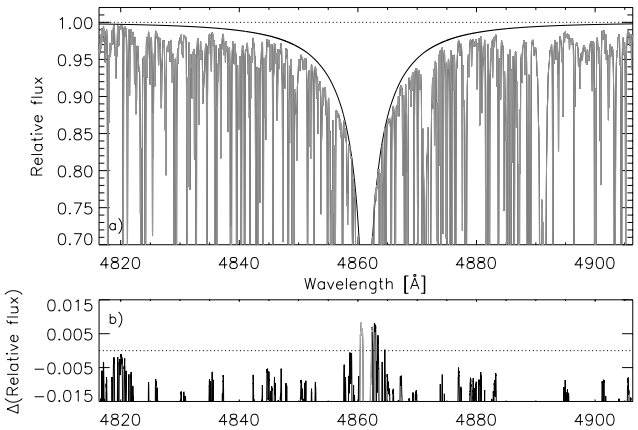


**Fig. 7.** Same as Fig. 6 but now showing solar $H_\beta$ line.

showing the deviation between measurement and model prediction. Both models seem too hot, in the sense of producing too broad lines. For $H_\alpha$ the effective temperature determined with this approach would be almost 80K below the known solar $T_{\rm eff}$, for $H_\beta$ the error would be around −50 K.

The higher series members are inadequate to determine the temperature of solar metallicity stars because, as can be seen already with $H_\beta$ in Fig. 7 it is almost impossible to determine the exact continuum for those lines.

The question now arises whether our MAFAGS-OS temperature structure is deficient by up to 80 K or whether we have deficiencies in the theories determining the shape of the lines considered.

Turning back to Fig. 18 of Paper I, a temperature structure 80 K different from the one used would hardly produce an overall match of measurement and predicted solar flux of the quality shown. Furthermore, Fig. 8 shows the situation using the same broadening theory as in Fig. 6 but now for the MAFAGS-ODF model. Although this fit is better than the one using our OS model, there is still a significant difference between theory and measurement, translating to an error in effective temperature of ≈−25 K. This was already described by Fuhrmann et al. (1997). This means that our MAFAGS-OS

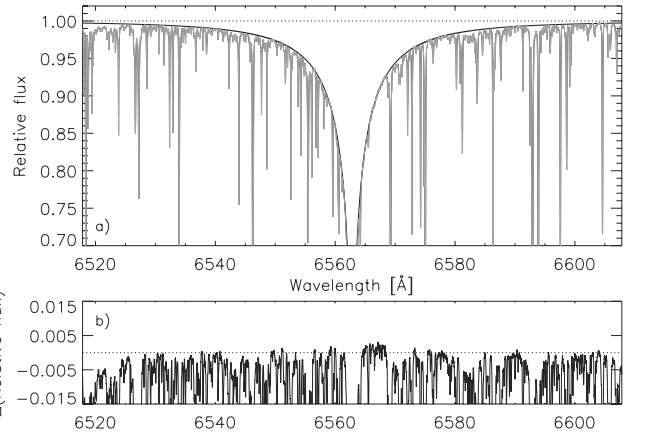


**Fig. 8.** Same as Fig. 6, now using the MAFAGS-ODF model atmosphere.

calculations show not a new but an increased discrepancy between theory and measurement.

### 3.2.1. Quantum mechanical treatment of resonance broadening according to Ali & Griem

Trusting our model as it is supported by the very good overall reproduction of the solar flux distribution and colors, we turn our attention to the theory of resonance broadening in the quantum mechanical treatment presented by Ali & Griem (1965) (furthermore AG65).

The basic idea of AG65 is to calculate the quantum mechanical interaction of two atoms connected via dipole-dipole and dipole-quadrupole interaction. More importantly, note their method of treating the transition from one perturbing atom to the physical situation of many perturbers by the simple integration over all single process *effects*.

Using this energy-transfer type of model in this way to generalise the problem from the single to the multi partner interaction should be critically reviewed. They proceed in this manner because the straightforward way of building up a total perturbing field $V_{\rm tot}$ contributed by all atoms in reach and solving this problem instead of the single perturber problem has no apparent solution. This fact was noticed and critically reviewed by Breene (1961, see p. 224) discussing a similar approach to solve the resonance broadening problem studied by Furssow & Wlassow (1936).

From this point of view the solution of AG65 represents a positive interference of the fields $V_i$ emerging from all perturbing atoms.

### 3.2.2. A possible cure for the Balmer lines

Seizing the idea that the Ali & Griem (1965) result, assuming all perturbers to be "in phase" as viewed from the perturbed atom, may well overestimate the situation we will now study the resulting profile functions adding a scaling factor to the AG65 theory. This is of cause a zero order approach, justified by the fact that we intend to carry out our analysis *strictly differential with respect to the Sun*. This approach will have to be

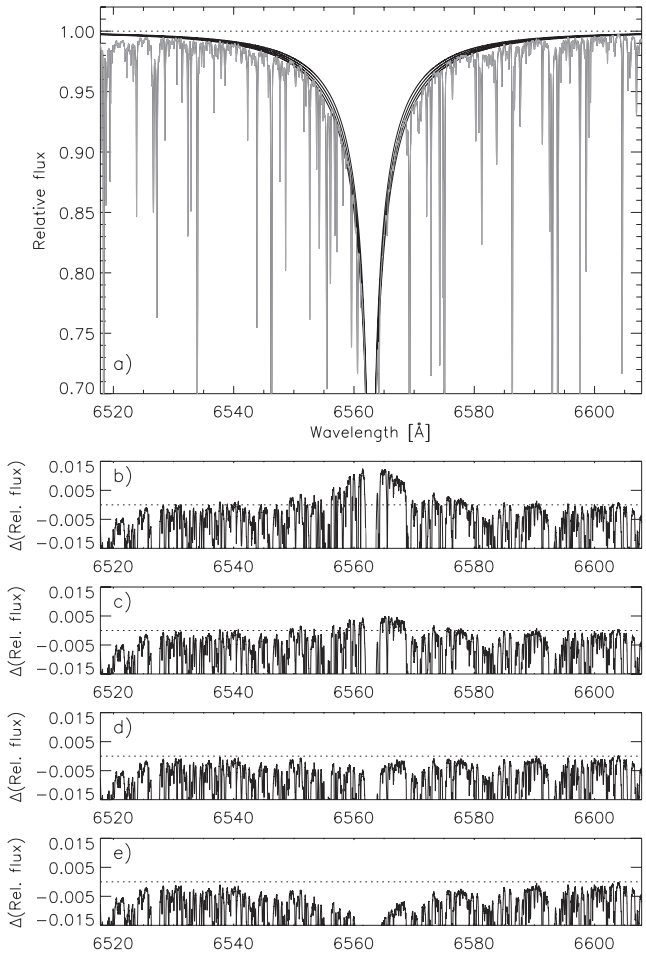


**Fig. 9.** Solar $H_\alpha$ line. **a)** Kitt Peak Solar Flux Atlas (grey), theoretical profiles using MAFAGS-OS (black),from top to bottom: AG-theory scaled by 0.4, AG65 scaled by 0.6, AG65 scaled by 0.8 and AG unscaled. **b)** Difference between theoretical and observed profile for unscaled model. **c)** Same as b) but AG65 scaled by 0.8. **d)** Same as b) but AG65 scaled by 0.6. **e)** Same as b) but AG65 scaled by 0.4.

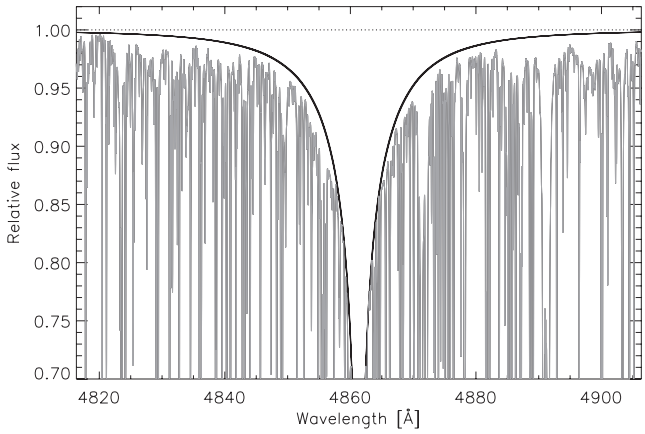


**Fig. 10.** Same as Fig. 9a but showing solar $H_\beta$ line.

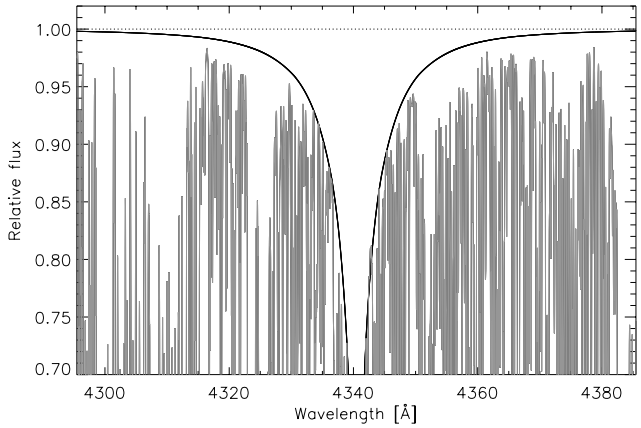


**Fig. 11.** Same as Fig. 9a but showing solar $H_\gamma$ line.

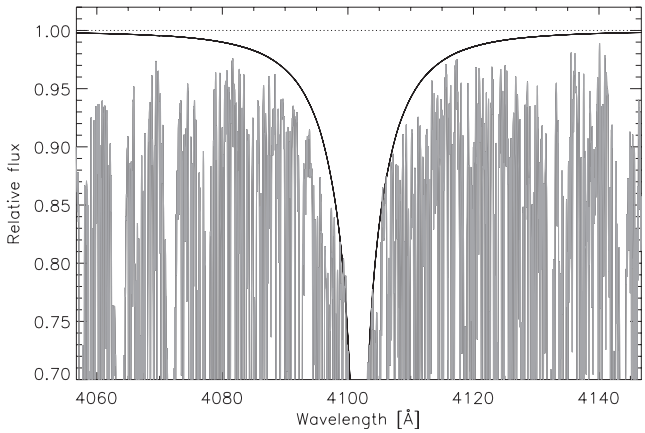


**Fig. 12.** Same as Fig. 9a but showing solar $H_\delta$ line.

tested against other stars and will have to show whether it is applicable compared to stellar evolution requirements and astrometric measurements. In general, scaling AG65 follows the same approach as the commonly accepted measurement of astrophysical $gf$ and $C_6$ values that is often used to determine metal abundances.

Figure 9 presents the results for the Balmer line $H_\alpha$ using scaling factors of 1.0, 0.8, 0.6 and 0.4 to the resonance broadening part of the line profile. It is obvious that for a scaling factor slightly above 0.6 (Fig. 9b an almost perfect fit to the observed solar spectrum is obtained over the whole spectral range of the line.

Figures 10–12 show the same plot as Fig. 9a but for the higher members of the Balmer series up to $H_\delta$. From these figures it can be seen, as already shown in Fig. 5, that the influence of resonance broadening becomes more and more miniscule towards higher series members, and that a difference in the quality of the fits shown cannot be evaluated.

From these studies we choose the correction factor for the scaling of the resonance broadening part in our Balmer line profiles to be 0.63.

The numerical value chosen to correct AG65 theory is of only subordinate meaning because its value depends on the detailed structure of the solar model used and therefore on the chosen theory and efficiency of convection.

Figures 13 and 14 show the difference in temperature determination for the the Balmer lines $H_\alpha$ and $H_\beta$ for both a solar metallicity and a metal-poor ([M/H] = −2.0) main

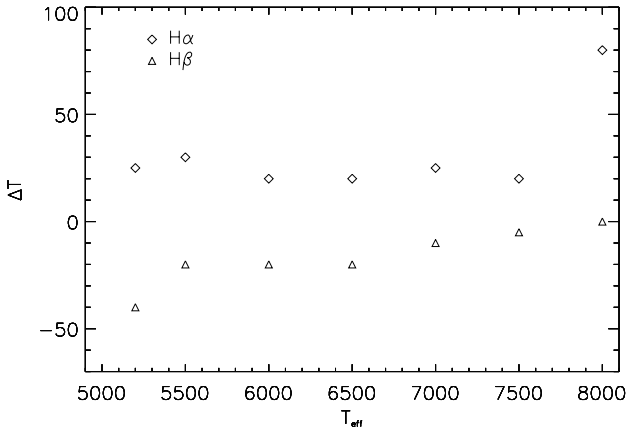


**Fig. 13.** Difference between MAFAGS-ODF model without Balmer line correction and MAFAGS-OS model including Balmer line correction for a solar metallicity main sequence. $\Delta T > 0$ indicates that the OS model measures a higher temperature.

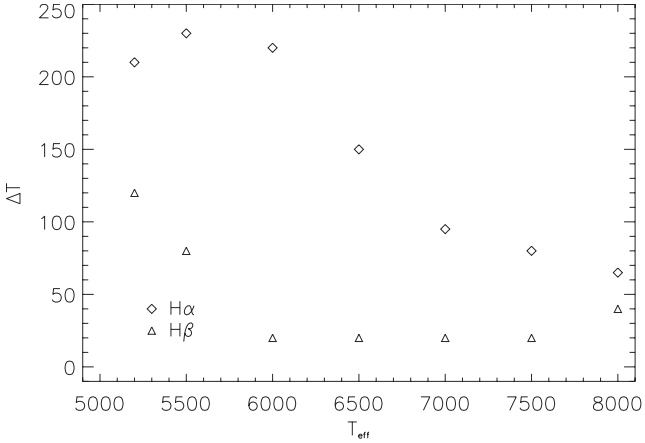


**Fig. 14.** Same as Fig. 13 but for a [M/H] = −2.0 metal-poor main sequence.

sequence. Although the change for solar metallicity stars are small, it is an impressing fact that the difference of ≈20–30 K that should be expected for the solar $H_\alpha$ line matches the difference found in the very detailed analysis of Fuhrmann et al. (1997) for this line. The far greater changes of measured temperatures for metal-poor stars will be discussed when we study Groombridge 1830 and HD 19445.

### 3.3. Procyon

Turning to our first, often-studied standard star, Fig. 15 shows the MAFAGS-ODF based uncorrected Balmer line profiles for $H_\alpha$ using the stellar parameters of Fuhrmann et al. (1997), i.e.:

$$\begin{aligned} T_{\rm eff} &= 6470\ {\rm K} \\ \log(g) &= 4.00 \\ [{\rm Fe/H}] &= 0.01 \\ \xi_{\rm micro} &= 2.09\ {\rm km\ s^{-1}} \end{aligned}$$

This plot, and all further plots of this type show the observed Balmer line (grey) and the model prediction (black) in Fig. a. Figure b shows the difference between model prediction and measurement. As the most interesting part of the line for temperature determination is the region between ≈0.98 and ≈0.85 times the continuum level we only display the line down to 0.7. Furthermore the region below 0.7 may well have a significant contribution of opacity formed in depth ranges outside $\log(\tau) = -4.0$, i.e parts of the atmosphere that are not properly modeled. Therefore the region below 0.7 times the continuum is displayed in grey in Fig. b.

Remaining uncertainties in the observational data must be kept in mind when knowing that our observations, carried out with the Foces spectrograph, are normalized *manually* in a procedure described by Fuhrmann et al. (1997). While this can be done with good accuracy for metal-poor, thus less blended stellar spectra, it becomes difficult for solar metallicity objects. Within one spectrum it turns out that the less blended region around $H_\alpha$ is much easier to process that the more line crowded region around $H_\beta$. While we expect the uncertainty of

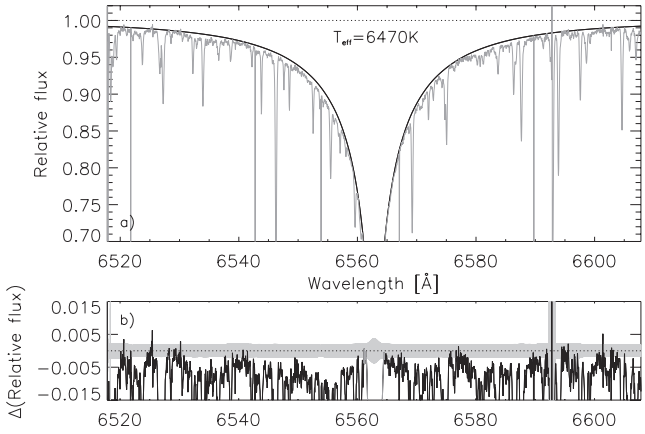


**Fig. 15.** Procyon: $H_\alpha$ line calculated using MAFAGS-ODF and **uncorrected** AG65 theory. **a)** Measurement (full grey line) and theory (full black line). **b)** Difference between measurement and theory. In addition, the expected photon and readout noise for the observed spectrum is displayed as shaded gray surface around the Δ(Relative flux) = 0 line.

Procyon's continuum to be less than 0.2% for $H_\alpha$, the situation for $H_\beta$ does not allow the continuum to be determined better than on a 0.5% level. For metal-rich stars $H_\beta$ is therefore only good as a confirmation of the temperature determined using the $H_\alpha$ line or to reveal large inconsistencies between $H_\alpha$ and $H_\beta$ temperatures respectively.

Turning to MAFAGS-OS models with corrected AG65 resonance broadening profiles we present the Balmer line spectrum calculated in Fig. 16. For $T_{\rm eff} = 6480$ K we achieve a very good fit for $H_\alpha$. The quality of this fit slightly exceeds that of the ODF model with unchanged AG65 line broadening (Fig. 15).

$H_\beta$ leads to a temperature determination of $T_{\rm eff} = 6460$ K for the MAFAGS-OS model.

We finally adopt $T_{\rm eff} = 6470$ K for Procyon using our new MAFAGS-OS models and the changed AG65 theory, an identical effective temperature as is found for MAFAGS-ODF models without changing AG65.

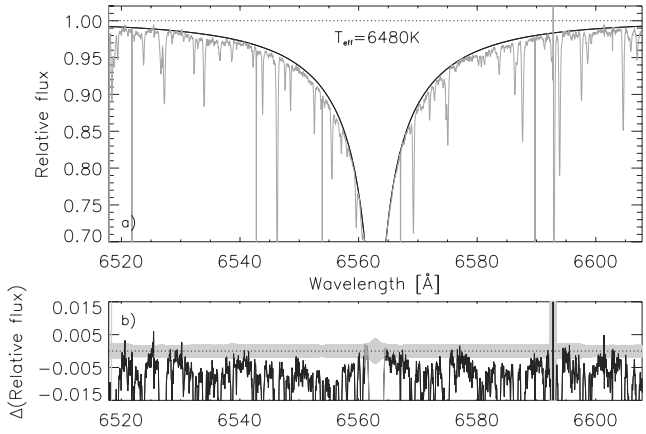


**Fig. 16.** Procyon: $H_\alpha$ line calculated using MAFAGS-OS and **corrected** AG65 theory.

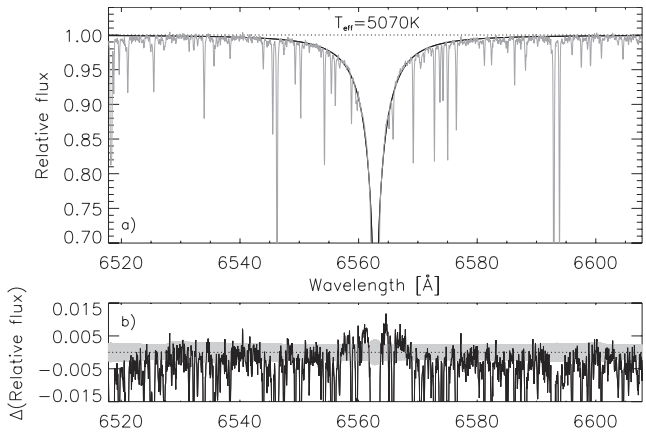


**Fig. 17.** Groombridge 1830: $H_\alpha$ line calculated using MAFAGS-ODF and **uncorrected** AG65 theory. **a)** Measurement (full grey line) and theory (full black line). **b)** Difference between measurement and theory. In addition, the expected photon and readout noise for the observed spectrum is displayed as shaded gray surface around the Δ(Relative flux) = 0 line.

### 3.4. Groombridge 1830

Turning to the metal-poor main sequence star Groombridge 1830 we start our comparison of Balmer line profiles based on the ODF analysis of Korn et al. (2003) and Korn (2002). These authors use MAFAGS-ODF during their iron NON-LTE work. The stellar parameters determined by Korn et al. (2003) for Groombridge 1830 are:

$$\begin{aligned} T_{\rm eff} &= 5070\ {\rm K} \\ \log(g) &= 4.66 \\ [{\rm Fe/H}] &= -1.35 \\ \xi_{\rm micro} &= 0.95\ {\rm km\ s^{-1}}. \end{aligned}$$

Figure 17 shows MAFAGS-ODF based AG65 Balmer line profiles for this star. The line most important for stellar effective temperature determination, $H_\alpha$, shows discrepancies between theory and observation. Starting from a relative flux of ≈0.96 to lower relative fluxes the theoretical profile overestimates the measured opacity.

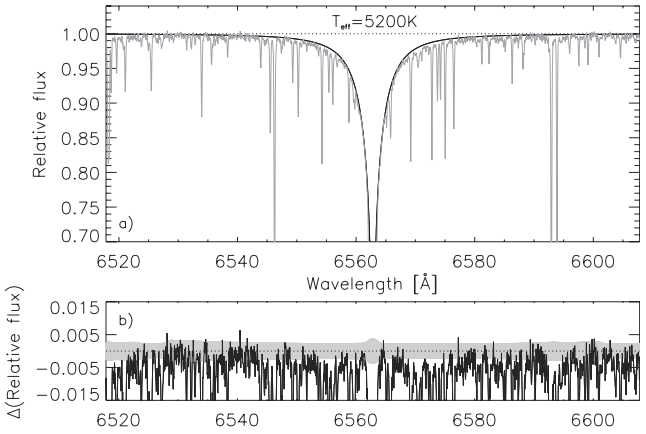


**Fig. 18.** Groombridge 1830: $H_\alpha$ line calculated using MAFAGS-OS and **corrected** AG65 theory.

**Table 2.** Different temperature determinations for Groombridge 1830.

| Author | $T_{\rm eff}$ | Method |
|---|---|---|
| Thévenin & Idiart (1999) | 4990 | $B-V$ |
| Alonso et al. (1996) | 5029 | IRFM |
| Korn et al. (2003) | 5070 | Balmer |
| Fuhrmann (1998) | 5110 | Balmer |
| Gratton et al. (1996) | 5124 | IRFM |
| Smith et al. (1992) | 5170 | Excitation equilibrium |
| Weiss & Schlattl (2000) | 5184 | Stellar evolution |
| This work | 5200 | Balmer |

Turning to our new MAFAGS-OS models together with corrected AG65 profile functions we present the comparison of measured and calculated Balmer line profiles in Fig. 18. The line is well reproduced by theoretical predictions, showing a significantly higher temperature of $T_{\rm eff}$ = 5200 K, a fact that could be expected looking at Fig. 14. $H_\beta$ confirms this temperature. The influence of this significant change in temperature on the stellar mass, age and parallax determination will be discussed in Sect. 5.

Table 2 shows a sample of temperature determinations done by different authors using different methods. A systematic difference within these determinations of $T_{\rm eff}$ corresponding to the method used cannot be found. It is obvious from the previous chapter that the changed AG65 theory will produce higher temperatures for metal-poor stars than the unchanged theory of resonance broadening does. Within these temperature determinations our value of $T_{\rm eff}$ = 5200 K is the highest, yet it cannot be called outstanding. In anticipation of Sect. 5 the temperature determination of Weiss & Schlattl (2000) is worth a closer look. Based on the requirements of stellar evolution his $T_{\rm eff}$ matches our measurement very closely, a fact that supports our high value of effective temperature for Groombridge 1830.

### 3.5. HD 19445

In analogy to the previously discussed stars we start with the comparison of MAFAGS-ODF based Balmer line profiles

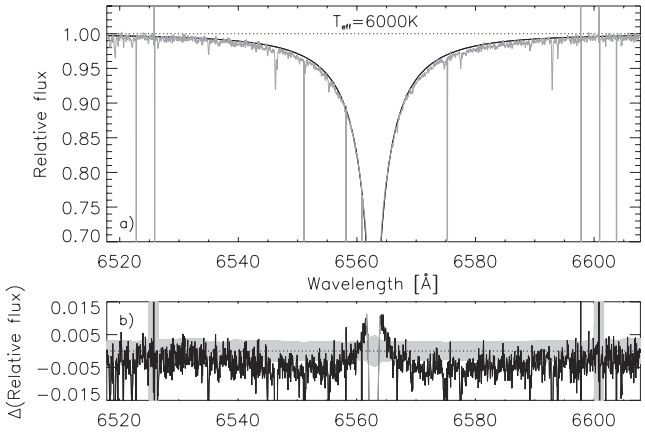


**Fig. 19.** HD 19445: $H_\alpha$ line calculated using MAFAGS-ODF and **uncorrected** AG65 theory. **a)** Measurement (full grey line) and theory (full black line). **b)** Difference between measurement and theory. In addition, the expected photon and readout noise for the observed spectrum is displayed as shaded gray surface around the Δ(Relative flux) = 0 line.

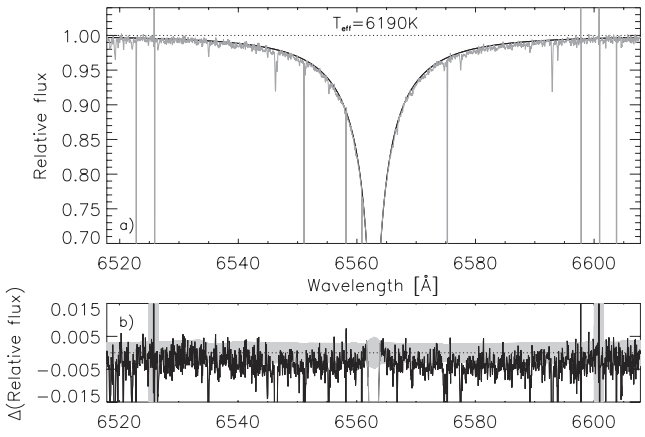


**Fig. 20.** HD 1445: $H_\alpha$ line calculated using MAFAGS-OS and **corrected** AG65 theory.

using the unchanged AG65 theory. In order to have comparable conditions we again take the MAFAGS analysis of Korn et al. (2003) and Korn (2002):

$$\begin{aligned} T_{\rm eff} &= 6032\ {\rm K} \\ \log(g) &= 4.40 \\ [{\rm Fe/H}] &= -2.08 \\ \xi_{\rm micro} &= 1.75\ {\rm km\ s^{-1}}. \end{aligned}$$

Figure 19 shows the measured flux and MAFAGS-ODF model prediction. It is obvious that the predicted $H_\alpha$ profile poorly fits the measured spectrum.

Turning to Fig. 20 we present our MAFAGS-OS model predictions together with the changed AG65 theory. The fit for $H_\alpha$, leading to $T_{\rm eff}(H_\alpha) = 6190$ K is very good, removing the deficiencies that are apparent in Fig. 19. $H_\beta$ leads to $T_{\rm eff}(H_\beta) = 6150$ K. As a weighted mean, with $H_\beta$ having half the weight of $H_\alpha$ we determine $T_{\rm eff} = 6176$ K for HD 19445.

Comparing our results to other authors, Table 3 shows that again the photometric work of Thévenin & Idiart (1999) is farthest from our own measurement, while

**Table 3.** Different temperature determinations for HD 19445.

| Author | $T_{\rm eff}$ | Method |
|---|---|---|
| Thévenin & Idiart (1999) | 5860 | $B-V$ |
| Fuhrmann (1998) | 6016 | Balmer |
| Korn et al. (2003) | 6032 | Balmer |
| Alonso et al. (1996) | 6050 | IRFM |
| Gratton et al. (1996) | 6066 | IRFM |
| Weiss & Schlattl (2000) | 6122 | Stellar evolution |
| This work | 6176 | Balmer |

Weiss & Schlattl (2000) is closest with effective temperature defined by the requirements of stellar evolution. As for Groombridge 1830 the effective temperature determined using opacity sampling type models and changed AG65 resonance broadening is much higher than for ODF type models with unchanged AG65. We refer to Sect. 5 for the influence of this change in $T_{\rm eff}$ on the stellar mass, age and distance.

## 4. Stellar parameters

After having described how we determine the stellar effective temperature we will turn to some other parameters used to characterise our stellar objects. The parameters *metallicity* [Me/H], photospheric *gravity* $\log(g)$, *microturbulent velocity* $\xi$ and *alpha element enhancement* [$\alpha$/Fe] are used to define the basic properties of our stars.

To restrict ourselvs to a low number of parameters is of course a simplification. In principle many more parameters are needed to define the properties of stellar objects. Individual element abundances [X/Fe] for example do influence the spectral properties of our objects. Opacity sampling puts us in the position to account for all these individual abundances. For the tests provided in this paper we restrict ourself to alpha element enhancement, knowing that this is below the possibilities of our model. The treatment of individual element abundances will become extremely valuable when turning to chemical peculiar stars that differ significantly from the *scaled solar mixture*, such as for example Ap stars.

The procedure of measuring the above stated parameters follows closely the iterative method described by Fuhrmann et al. (1997) and Fuhrmann (1998). This method is based on the idea of working differentially with respect to the star we know best, our Sun.

In the following we will give a brief summery of how the fundamental parameters are determined:

**Metallicity.** The overall metallicity is equated to the iron abundance of the star. From the view of opacity iron is the most prominent element in the photosphere of our objects (see Paper I). As shown in Fig. 21 for the Sun Fe II is the dominating ionization stage in our stars. Moreover Fe II is less influenced by deviations from local thermodynamical equlibrium (see Gehren et al. 2001 and Korn et al. 2003). We therefore use the Fe II abundance as overall metallicity [M/H]. Only lines with equivalent widths below 130 mÅ are used for our analysis.

**Table 4.** Stellar parameters for Procyon, Groombridge 1830 and HD 19445. $T_{\rm eff}$ determined using Balmer lines, the error is estemated from the quality of the fit for $H_\alpha$ and $H_\beta$; $\log(g)$ determined from Mg Ib triplet, the error is set to 0.1 as a raw estimate of the insecurities $\log(g)$ of the input physics and data; [Fe II/H], i.e. the metallicity is determined from profile fits, the error is defined by the standard deviation within the sample of lines used to determine [Fe II/H]. The number in brackets states the number of lines used for this measurement; [Fe I/H] and [Mg I/Fe I] same as [Fe II/H]; $\xi$ determined by forcing all Fe II lines to lead to one consistent abundance, the error is set to 0.1 if more than 10 lines where used and to 0.2 if less than ten lines were used to determine [Fe II/H].

| Name | $T_{\rm eff}$ [K] | $\log(g)$ | [Fe II/H] (# lines) | [Fe I/H] (# lines) | [Mg I/Fe I] (# lines) | $\xi$ [km/s] |
|---|---|---|---|---|---|---|
| Procyon | $6470 \pm 50$ | $3.96 \pm 0.10$ | $+0.00 \pm 0.03$ (16) | $-0.11 \pm 0.06$ (36) | $+0.03 \pm 0.06$ (3) | $2.10 \pm 0.1$ |
| Groombridge 1830 | $5200 \pm 40$ | $4.69 \pm 0.10$ | $-1.29 \pm 0.02$ (5) | $-1.27 \pm 0.04$ (28) | $+0.28 \pm 0.03$ (3) | $1.25 \pm 0.2$ |
| HD 19445 | $6176 \pm 50$ | $4.47 \pm 0.10$ | $-1.88 \pm 0.03$ (7) | $-1.89 \pm 0.08$ (14) | $+0.33 \pm 0.01$ (3) | $1.31 \pm 0.2$ |

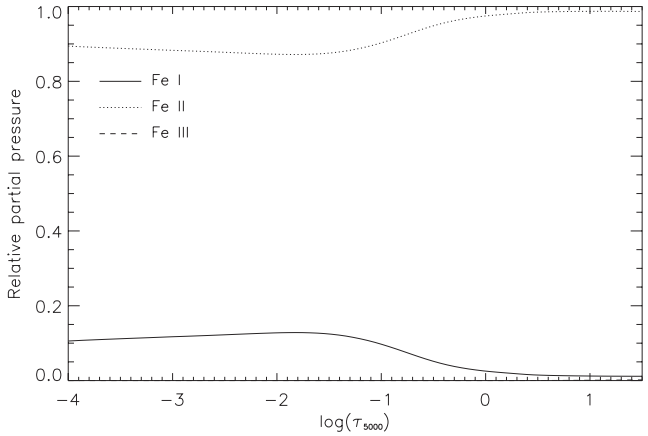


**Fig. 21.** Relative partial pressures of iron in the solar photosphere. Note that Fe III is not notably present in the solar atmosphere.

We work differentially with respect to the Sun, i.e. atomic line data is defined by fitting the solar spectrum using MAFAGS-OS. As we intend to do spectroscopy and use as much information from our spectra as possible we use solely profile fits and do not rely on integrated information such as equivalent widths.

**Gravity.** The photospheric gravity is determined using the wings of the strong Mg Ib triplet.

**Microturbulenze.** We use one single microturbulence throughout the whole atmosphere. This microturbulence is determined by the requirement that all Fe II lines of different strength lead to a consistent abundance.

**Alpha enhancement.** The overabundance of the alpha elements O, Ne, Mg, Si, S and Ca are accounted for in our model. Some of these elements have low ionization energies and contribute not only through their own opacity, but through a change of the electron pressure to the atmospheric structure. Ne, Mg, Si, S and Ca are assigned the measured Mg overabundance, whereas oxygen is assigned 1.5 times the magnesium overabundance. This is due to the fact that Mg seems to converge into an overabundance of [Mg/Fe] $\approx$ 0.4 for very metal-poor stars (see Fuhrmann 1999) whereas oxygen trends towards [O/Fe] $\approx$ 0.6 (see Reetz 1999).

The parameter[$\alpha$/Fe] is assigned the magnesium abundance [Mg/Fe] in our analysis. In order to compare equipollent partners the abundance [Mg I/Fe I] is given for our stars.

**Table 5.** Literature values for Procyon stellar parameters: EAGLNT93 Edvardsson et al. (1993), FUHR97 Fuhrmann et al. (1997) and KO03 Korn et al. (2003).

| Author | $T_{\rm eff}$ | $\log(g)$ | [Fe/H] | $\xi$ |
|---|---|---|---|---|
| EAGLNT93 | $6704 \pm 100$ | $4.03 \pm 0.10$ | $+0.08 \pm 0.10$ | 2.42 |
| FUHR97 | $6470 \pm 80$ | $4.00 \pm 0.10$ | $+0.01 \pm 0.07$ | 1.91 |
| KO03 | $6510 \pm 60$ | $3.96 \pm 0.02$ | $-0.03 \pm 0.04$ | 1.83 |

Table 4 lists the parameters determined for the three stars studied for this paper[4].

After having presented the stellar parameters for our stars we will now compare them to other authors.

### 4.1. Procyon

Except for Edvardsson et al. (1993) who find a much higher effective temperature our measurements for Procyon are well consistent with the analysis shown in Table 5. Fuhrmann (1998) and Korn et al. (2003) use the ODF version of MAFAGS for their studies whereas Edvardsson et al. (1993) use a partly OS based model atmosphere code.

All three authors find an inconsistency between [Fe I/H] and [Fe II/H], reaching from 0.06 Dex (Edvardsson et al. 1993) up to 0.17 Dex (Fuhrmann et al. 1997) an inconsistency that is not resolved by our model leading to a difference between [Fe I/H] and [Fe II/H] of 0.11 Dex.

### 4.2. Groombridge 1830

Having a much higher temperature for Groombridge 1830 we expect the other parameters to change due to the changed thermal structure of the photosphere. It is indeed surprising how small these changes are. Due to its higher temperature, the metallicity changes towards higher values in fact a change of 0.06 Dex compared with Fuhrmann (1998) and Korn et al. (2003) (see Table 6), both using the ODF version of MAFAGS is significant but small.

[4] The errors, given for [Fe I/H] are always bigger than those of [Fe II/H]. This is due to the fact that the microturbulence $\xi$ is determined for Fe II. It would lead to slightly different values for Fe I, i.e. Fe I abundances show a slope with the equivalent width leading to larger standard deviation.

**Table 6.** Literature values for Groombridge 1830 stellar parameters: SMI92 Smith et al. (1992), FUHR98 Fuhrmann (1998) and KO03 Korn et al. (2003).

| Author | $T_{\rm eff}$ | $\log(g)$ | [Fe/H] | $\xi$ |
|---|---|---|---|---|
| SMI92 | $5170 \pm 70$ | $4.5 \pm 0.1$ | $-1.30 \pm 0.06$ | 1.45 |
| FUHR98 | $5110 \pm 80$ | $4.66 \pm 0.10$ | $-1.35 \pm 0.10$ | 0.85 |
| KO03 | $5070 \pm 60$ | $4.66 \pm$ [1] | $-1.35 \pm 0.03$ | 0.95 |

[1] No value stated.

**Table 7.** Literature values for HD 19445 stellar parameters: FUHR98 Fuhrmann (1998),TI99 Thévenin & Idiart (1999) and KO03 Korn et al. (2003).

| Author | $T_{\rm eff}$ | $\log(g)$ | [Fe/H] | $\xi$ |
|---|---|---|---|---|
| FUHR98 | $6016 \pm 80$ | $4.38 \pm 0.10$ | $-1.95 \pm 0.07$ | 1.35 |
| TI99 | $5860 \pm$ [1] | $4.42 \pm$ [1] | $-1.88 \pm$ [1] | 1.4 |
| KO03 | $6032 \pm 60$ | $4.40 \pm$ [1] | $-2.08 \pm 0.05$ | 1.75 |

[1] No value stated.

Our value for the microturbulent velocity $\xi$ is between the lower values of Fuhrmann (1998) and Korn et al. (2003) and the higher value of Smith et al. (1992). Because all authors give an uncertainty for $\xi$ of $0.1 \cdots 0.2$ km s$^{-1}$ our value of $\xi = 1.25$ is still consistent with the other measurements.

### 4.3. HD 19445

As it was already seen for Groombridge 1830 the even higher changes in effective temperature lead to an increase of metallicity for HD 19445 as compared with the ODF based MAFAGS studies of Fuhrmann (1998) and Korn et al. (2003). Furthermore we find an increased photospheric gravity. Although this increase is still within the error bars of the determinations presented in Table 7 it will affect the age and mass determination of HD 19445.

The microturbulence detemined in this work is close to the values of Thévenin & Idiart (1999) and Fuhrmann (1998) but differs from that of Korn et al. (2003).

## 5. Stellar masses, ages and distances

Having determined the basic parameters of our programme stars we will now use these data to evaluate stellar masses, ages and distances. As all three stars are within the reach of the Hipparcos sattellite, accurate distance data is available for these three objects and will be compared to the spectroscopic parrallaxes determined. Table 8 presents the results for the three programme stars.

Beside the comparison with high precision astrometric data of the Hipparcos project another important test for our metal-poor stars Groombridge 1830 and HD 19445 will be the consistency with recent *age of the Universe* determinations. Recent determinations of the age of the Universe ($t_0$) that are based on cosmological constraints and high precision measurements of the Hubble constant $H_0$ on the one hand and globular cluster ages on the other are tabulated in Table 9. We have to state very clearly and explicitly that the determination of stellar ages becomes almost impossible for cool, low-mass, main-sequence stars. Groombridge 1830 turns out to be an unevolved star of low mass whose error-bars allow ages between 0 and 30 Gyr. We therefore do not intend to claim the ability to detemine the age of Groombridge 1830. Rather, we show its position in the $\log(T_{\rm eff}) - \log(g)$ plane, and we will show an improved consistency with evolutionary constraints. As far as HD 19445 is concerned its more evolved state and higher mass allow an – at least rough – age determination.

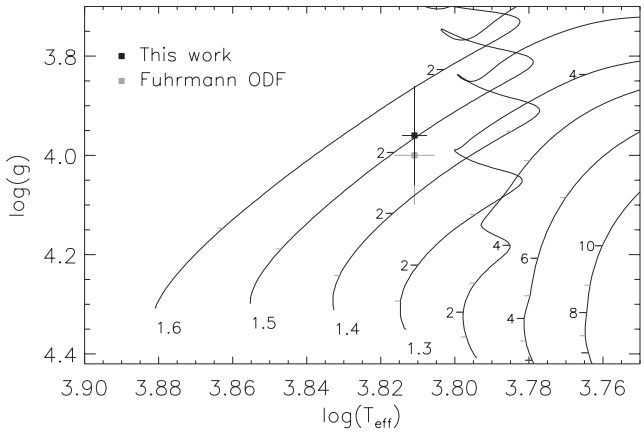


**Fig. 22.** Procyon: evolutionary tracks for [Fe/H] = 0.0 and [$\alpha$/Fe] = 0.0. The tickmarks along the tracks are in 1 Gyr distance.

In order to show the difference of our measurements using MAGAGS-OS together with the scaled AG65 theory of resonance broadening and ODF-type models, we choose Fuhrmann et al. (1997) and Fuhrmann (1998) to compare our data with. This choice is made because Fuhrmann uses the ODF version of MAFAGS and his method of parameter determination is identical with this work.

### 5.1. Procyon

Based on our stellar parameters for Procyon presented in Table 4 we use the VandenBerg et al. (2000) stellar evolution models to determine its mass and age. Figure 22 shows the position of Procyon in the $\log(T_{\rm eff}) - \log(g)$ plane, together with the evolutionary models for stars of masses from 1.6 $\mathcal{M}_\odot$ to 0.9 $\mathcal{M}_\odot$. Procyon turns out to lie directly on the 1.50 $\mathcal{M}_\odot$ track having an age of $\approx$2.1 Gyr. Plotted in grey is the position of Procyon based on Fuhrmann et al. (1997) ODF-based parameters. As already shown in Tables 4 and 5 the differences between Fuhrmann et al. (1997) and our work are small, a fact that translates directly into small differences in Procyon's evolutionary state.

Based on our measurement of Procyon's mass it is now possible to calculate its spectroscopic distance, which turns out to be $d_{\rm sp} = 3.50$ pc, in perfect agreement with Hipparcos astrometry.

**Table 8.** Masses, approximate ages and distances for Procyon, Groombridge 1830 and HD 19445. The last three columns give astrometric (Hipparcos) distance, spectroscopic distance and the relative difference between the two distance measurements.

| Name | $T_{\rm eff}$ [K] | $\log(g)$ | [M/H] | Mass [$\mathcal{M}_\odot$] | Age [Gyr] | $d_{\rm hip}$ [pc] | $d_{\rm sp}$ [pc] | $\Delta(d)$ |
|---|---|---|---|---|---|---|---|---|
| Procyon | $6470 \pm 50$ | $3.96 \pm 0.10$ | +0.00 | 1.50 | 2.1 | 3.50 | 3.50 | 0.0% |
| Groombridge 1830 | $5200 \pm 40$ | $4.69 \pm 0.10$ | −1.29 | 0.66 | 7 | 9.16 | 9.33 | +1.9% |
| HD 19445 | $6176 \pm 50$ | $4.47 \pm 0.10$ | −1.88 | 0.73 | 13 | 38.68 | 39.44 | +1.9% |

**Table 9.** Age of the Universe determinations.

| Author | $t_0$ [$10^9$ yr] | Method |
|---|---|---|
| Carretta et al. (2000) | $12.9 \pm 2.9$ | Globular clusters |
| Mould (2000) | $14.3 \pm 1.4$ | $H_0$ |

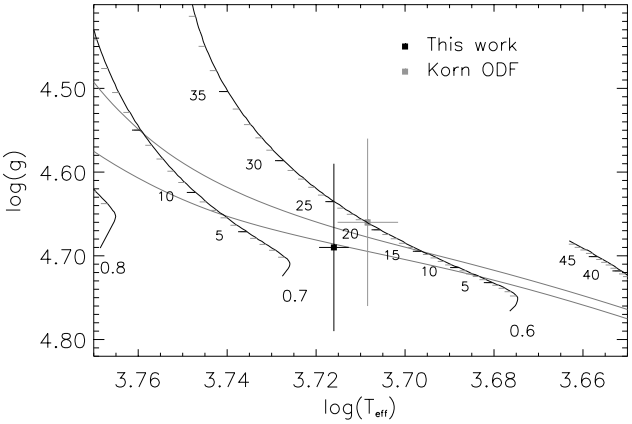


**Fig. 23.** Groombridge 1830: Evolutionary tracks interpolated to [Fe/H] = −1.29 and [$\alpha$/Fe] = +0.29. In addition two isochrones are plotted for 7.5 and 15 Gyr.

### 5.2. Groombridge 1830

Using VandenBerg et al. (2000) tracks that are interpolated to fit the measured data for [M/H] and [$\alpha$/Fe] we present the position of Groombridge 1830 in the $\log(T_{\rm eff}) - \log(g)$ plane in Fig. 23. Tracks for 0.8 $\mathcal{M}_\odot$ down to 0.5 $\mathcal{M}_\odot$ are plotted. It becomes obvious from Fig. 23 that for unevolved objects near to the zero age main sequence an age and mass determination becomes extremely difficult due to the enourmous influence of the error bars (mainly in $\log(g)$ direction) on the accuracy of the determined mass and age. Furthermore it becomes apparant that there is an enourmous deficiency between the ODF-position of Groombridge 1830 and the *allowed* region in the unevolved part of the main sequence of ages below 15 Gyr. This discrepancy was noticed by Cayrel et al. (1997) studying population II stars in the Hipparcos sample. One possible solution to solve this discrapancy is a change of the temperature scale for cool population II stars. In fact this is what MAFAGS-OS together with the scaled AG65 theory does. The OS-position of Groombridge 1830 is therefore in agreement with the VandenBerg et al. (2000) evolutionary model calculations.

We measure a mass of 0.66 $\mathcal{M}_\odot$ and an age of ≈7 Gyr for Groombridge 1830. The spectroscopic distance based on these

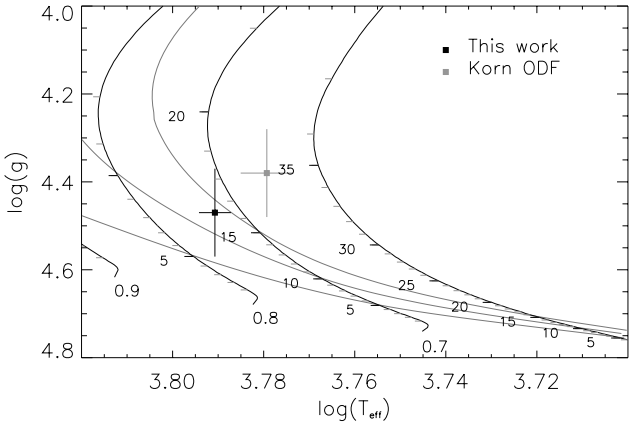


**Fig. 24.** HD 19445: Evolutionary tracks interpolated to [Fe/H] = −1.88 and [$\alpha$/Fe] = +0.33.In addition three isochrones are plotted for 5, 10 and 15 Gyr.

measurements is $d_{\rm sp}$ = 9.33 pc, being 1.9% further away than measured by Hipparcos. This good agreement of astrometric and spectroscopic distance increases our confidence that the mass – and age – of Groombridge 1830, although insecure for a star near the main sequence due to the error-bars, are well determined parameters.

Turning to the ODF-based parameters of Fuhrmann (1998) it is to be pointed out that plotting these data on the same diagram is a simplification due to the fact that other values for [M/H] and [$\alpha$/Fe] should be used. As these data do not differ too strongly, and to allow a simple comparison, we use this simplified method to show that with Fuhrmann (1998) ODF data the age of Groombridge 1830, measured to be >20 Gyr, is unreasonably high compared to the age of the Universe.

### 5.3. HD 19445

Based on interpolated VandenBerg et al. (2000) tracks HD 19445's position in the $\log(T_{\rm eff}) - \log(g)$ plane is presented in Fig. 24. Tracks for 0.9 $\mathcal{M}_\odot$ down to 0.6 $\mathcal{M}_\odot$ are plotted. Being more evolved than Groombridge 1830, the mass of HD 19445 can be better determined and turns out to be 0.73 $\mathcal{M}_\odot$; its age can be evaluated to be ≈13 Gyr. Knowing its mass, the spectrscopic distance of HD 19445 is found to be $d_{\rm sp}$ = 39.44 pc, 1.9% further away than measured by Hipparcos, whose error bar reaches ≈4% for these distances.

Again using the simplifications described above we use Fig. 24 to show the comparison with the Fuhrmann (1998) ODF analysis of HD 19445. The age of the star is again >20 Gyr for the ODF-type parameters and show the same problem as

Groombridge 1830 that was found to be a general problem in the studies of Cayrel et al. (1997). This inconsitency is again revealed by the OS-model. HD 19445 now has an age well below the age of the Universe, i.e. our OS type stellar parameters resolve the paradox of *a part being older than the lot*.

## 6. Discussion

After having introduced MAFAGS-OS in Paper I and having shown its validity to fit the solar flux distribution and colours we study the influence of the changed atmospheric structure in this second paper.

MAFAGS-OS, having a 10–60 K higher temperature in the important layers of the solar photosphere is shown to change the infrared flux of stars. This is mainly due to the fact that this new model uses Bautista (1997) cross sections for Fe I that are significantly larger than the hitherto most commonly used hydrogenic approximations. These changes in the IR flux will of course influence the so-called *infrared flux method* to determine stellar effective temperatures. As shown by Megessier (1994) this method does indeed strongly depend on the properties of the atmospheric model used, a fact that has to be taken into consideration when comparing effective temperatures determined using IR fluxes to other methods of effective temperature determination. It has also to be taken into account judging the absolute accuracy of this type of temperature measurement.

The changed solar temperature structure of MAFAGS-OS is also shown to require revisiting of Balmer line profiles in the Sun and stars. While MAFAGS-ODF models together with the Vidal et al. (1973) and Ali & Griem (1965) line broadening theory reproduced the Sun with an error of approximately 20 K, new MAFAGS-OS models increased this error to an intolerable level of up to 80 K as shown in Fig. 6. this problem would even increase using new data available from Barklem et al. (2000a) producing much *hotter* profiles than Ali & Griem (1965). A method of resolving these problems using a scaled theory of AG65 is presented. As we work differentially with regard to the Sun, a zero order approach of scaling AG65 data by 0.63 is chosen. This is justified looking at a questionable transition used by AG65 when changing from the one pertuber problem to the many pertubers problem (see Sect. 3.2.2).

This scaled theory, together with the MAFAGS-OS model is tested on three very different stars: The hot, solar metallicity star Procyon, the metal-poor, cool main sequence star Groombridge 1830 and the hot, metal-poor, moderately evolved star HD 19445. While the stellar parameters of Procyon are almost unchanged, the metal-poor stars show a significant increase of temperature. The quality of congruence between theoretical and observed Balmer line profiles is increased.

For the first member of the Balmer series $H_\alpha$ the fit quality is very good for all stars studied in this paper. This becomes even more important knowing that for stars of solar metallicity $H_\alpha$ is the only Balmer line for which the continuum can be determined with reasonable accuracy. In fact Balmer line temperatures for stars of solar (or higher) metallicity are mostly $H_\alpha$ temperatures.

The new model, together with an increased temperature for the metal-poor stars of our sample, influence the other stellar parameters to a certain degree. Stellar masses and ages determined using these parameters are found to be consistent with the *age of the Universe* determined using globular clusters and cosmological methods (see Sect. 5). The unreasonably high ages for Groombridge 1830 and HD 19445 of over 20 Gyr are lowered to ≈7 Gyr for Groombridge 1830 and ≈13 Gyr for HD 19445.

Studying population II stars of the Hipparcos sample Cayrel et al. (1997) noticed that, in order to achieve consistency, it is required to shift the tracks of VandenBerg 0.01 in $\log(T_{\rm eff})$. If we look at the changes the new model MAFAGS-OS, together with Bautista (1997) cross sections for Fe I and a changed AG65 theory applied to the effective temperatures of Groombridge 1830 and HD 19445, we find $\Delta \log(T_{\rm eff}) \approx 0.011$ for Groombridge 1830 and $\Delta \log(T_{\rm eff}) \approx 0.014$ for HD 19445. This remarkable agreement shows that our new model removes the discrepancy between observation and the evolutionary models that was noticed by Cayrel et al. (1997).

Spectroscopic distances calculated with data using MAFAGS-OS, the scaled AG65 theory and the resulting stellar masses are in very good agreement with Hipparcos astrometry.

Thus, the new MAFAGS-OS models, together with a changed theory of resonance broadening, fit the solar flux distribution, color and Balmer line profile. This allows the measurement of stellar parameters that turn out to be in excellent agreement with Hipparcos astrometry and resolves the paradox of stars being older than the Universe.

Remaining deficiencies can be found with the center to limb variation of the solar continuum (Paper I).

*Acknowledgements.* Thanks goes to T. Gehren, K. Fuhrmann and A. Korn for their help and useful discussions. Thanks to Constance who suffered from many "interesting" astronomical news and from me waking her in the middle of the night to announce that HD 19445 had become 7 billion years younger during the last 30 min.

## References

Ali, R., & Griem, H. 1965, Phys. Rev., 140, 1044
Alonso, A., Arribas, S., & Martinez-Roger, C. 1996, A&AS, 117, 227
Böhm-Vitense, E. 1958, Z. Astrophys., 46, 108
Barklem, P. S., Piskunov, N., & O'Mara, B. J. 2000a, A&A, 363, 1091
Barklem, P. S., Piskunov, N., & O'Mara, B. J. 2000b, A&A, 355, L5
Barklem, P. S., Stempels, H. C., Allende Prieto, C., et al. 2002, A&A, 385, 951
Bautista, M. A. 1997, A&AS, 122, 167
Bernkopf, J. 1998, A&A, 332, 127
Blackwell, D. E., & Lynas-Gray, A. E. 1998, A&AS, 129, 505
Blackwell, D. E., Petford, A. D., & Shallis, M. J. 1980, A&A, 82, 249
Blackwell, D. E., & Shallis, M. J. 1977, MNRAS, 180, 177
Breene, R. G. 1961, The Shift and Shape of Spectral Lines, ed. P. Dünnhaupt (Pergamon Press)
Canuto, V. M., & Mazzitelli, I. 1991, ApJ, 370, 295
Carretta, E., Gratton, R. G., Clementini, G., & Fusi Pecci, F. 2000, ApJ, 533, 215
Castelli, F., Gratton, R. G., & Kurucz, R. L. 1997, A&A, 318, 841
Cayrel, R., Lebreton, Y., Perrin, M.-N., & Turon, C. 1997, in ESA SP-402: Hipparcos – Venice'97, 219

Cayrel de Strobel, G., & Bentolila, C. 1989, A&A, 211, 324
de Strobel, G. C. 1985, in Calibration of Fundamental Stellar Quantities, IAU Symp., 111, 137
Edvardsson, B., Andersen, J., Gustafsson, B., et al. 1993, A&A, 275, 101
Fuhrmann, K. 1993, Ph.D. Thesis, Universitäts Sternwarte München
Fuhrmann, K. 1998, A&A, 338, 161
Fuhrmann, K. 1999, Ap&SS, 265, 265
Fuhrmann, K., Axer, M., & Gehren, T. 1993, A&A, 271, 451
Fuhrmann, K., Axer, M., & Gehren, T. 1994, A&A, 285, 585
Fuhrmann, K., Pfeiffer, M., Frank, C., Reetz, J., & Gehren, T. 1997, A&A, 323, 909
Furssow, W., & Wlassow, A. 1936, Physik Z. Sowjetunion, 10, 373
Gardiner, R. B., Kupka, F., & Smalley, B. 1999, A&A, 347, 876
Gehren, T., Korn, A. J., & Shi, J. 2001, A&A, 380, 645
Gratton, R. G., Carretta, E., & Castelli, F. 1996, A&A, 314, 191
Grupp, F. 2003, A&A, 412, 897
Grupp, F. 2004, A&A, 420, 289
Korn, A. J. 2002, Ph.D. Thesis, Universitäts Sternwarte München
Korn, A. J., Shi, J., & Gehren, T. 2003, A&A, 407, 691
Kurucz, R. L., Furenlid, I., & Brault, J. 1984, Solar flux atlas from 296 to 1300 NM, National Solar Observatory Atlas, Sunspot (New Mexico: National Solar Observatory)
Megessier, C. 1994, A&A, 289, 202
Megessier, C. 1998, in Fundamental Stellar Properties, IAU Symp., 189, 153
Mould, J. 2000, PASA, 17, 45
Perrin, M.-N., Cayrel de Strobel, G., & Dennefeld, M. 1988, A&A, 191, 237
Pfeiffer, M. J., Frank, C., Baumueller, D., Fuhrmann, K., & Gehren, T. 1998, A&AS, 130, 381
Reetz, J. 1999, Ap&SS, 265, 171
Schöning, T., & Butler, K. 1990, Private communications
Smith, G., Lambert, D. L., & Ruck, M. J. 1992, A&A, 263, 249
Spite, M. 1969, A&A, 1, 52
Thévenin, F., & Idiart, T. P. 1999, ApJ, 521, 753
VandenBerg, D. A., Swenson, F. J., Rogers, F. J., Iglesias, C. A., & Alexander, D. R. 2000, ApJ, 532, 430
Vidal, C., Cooper, J., & Smith, E. 1973, ApJS., 37
Weiss, A., & Schlattl, H. 2000, A&AS, 144, 487